China HT1 (HONGTU-1, also called PIESAT-1) SAR support within GAMMA Software

Urs Wegmüller, Christophe Magnard, Gamma Remote Sensing AG

Version 14-Jun-2024 (initial version)

1. INTRODUCTION

In this document the support provided in the GAMMA Software for the processing of data of the Chinese X-band SAR Constellation HT1 (Hongtu-1, also called PIESAT-1) is summarized. The HT1 multi-static SAR Constellation was launched in March 2023. It includes the active sensor (monostatic SAR) HT1-A and the three passive (multi-static) sensors HT1-B, HT1-C, and HT1-D.

In Section 2 the importing of the multi-static HT1 SLC data is described, followed by an assessment of the data characteristics, in Section 3. In Section 4, the multi-static DInSAR processing sequence is presented. The main result generated is a terrain height correction relative to a pre-existing DEM. In addition coherence and backscatter are discussed.

2. IMPORTING HT1 SLC DATA

2.1. Importing SLC data

A multi-static HT1 acquisition consists of the monostatic HT1-A SLC and the 3 bistatic HT1-B, HT1-C, and HT1-D SLCs. Both the mono- and bistatic SLCs are provided as a GeoTIFF with meta data in XML format, that can be read / imported using the program ***par_HT1_SLC***.

par_HT1_SLC H/HT1-A*/*.tiff H*/HT1-A*/*.xml A.20230905.slc.par A.20230905.slc 0*

As input, the GeoTIFF and the meta data XML files are indicated. The program generates the SLC binary data file, in SCOMPLEX or FCOMPLEX format, and the related SLC parameter file. The SLC can be visualized using

disSLC 20230403.slc 26088 1 - 1. .35 0

and the spectrum can be checked using

dismph_fft 20230403.slc 26088 1 0 1. .35 128 3 0

In the data set we had available the spectrum determined from the data and the Doppler Centroid information extracted from the metadata did not correspond to each other. So possibly we did not correctly interpret the information in the metadata, or this information is not correct. In any case the GAMMA ISP program *doppler_2d_SLC* could be used to estimate Doppler parameters and insert these into the SLC parameter file:

doppler_2d_SLC A.20230905.slc A.20230905.slc.par dop2d 0 2048 - 0 0 0 0

Based on our tests it seems estimating only the constant value and range dependence (without time dependence) seems sufficient. This estimate was done for all the 4 scenes and similar values were

found. As a test we deramped the data considering the estimated Doppler Centroid and found that this results in nicely centered spectra.

Remark 1: Based on offset fields determined between the mono-static reference SLC and the bi-static acquisitions we identified for the last lines azimuth offsets of 1 azimuth SLC pixel. A possible explanation might be a missing line in the raw data. To avoid degrading the quality of later processing steps we just deleted the bottom part of the reference SLC. Based on our limited experience (with just one scene) we recommend checking the HT1 SLCs for this kind of problem by calculating offset fields between the SLCs.

Remark 2: Using *ORB_filt_spline.py* we checked the state vectors. The standard deviation between the unfiltered and filtered values is small (< 2mm for each component). So it seems that the state vectors can be used as provided in the meta data.

Using the SLC we generate a backscatter image in slant range geometry using *multi_look* or *multi_look2*:

multi_look2 A.20230905.slc A.20230905.slc.par A.20230905.mli A.20230905.mli.par 3 2 5 4 1 2 7 2. 0.00002

ras_dB A.20230905.mli 8696 1 0 1 1 -10. 10. gray.cm A.20230905.mli.bmp 0 0

The mono-static HT1 backscatter image is shown in Figure 1.

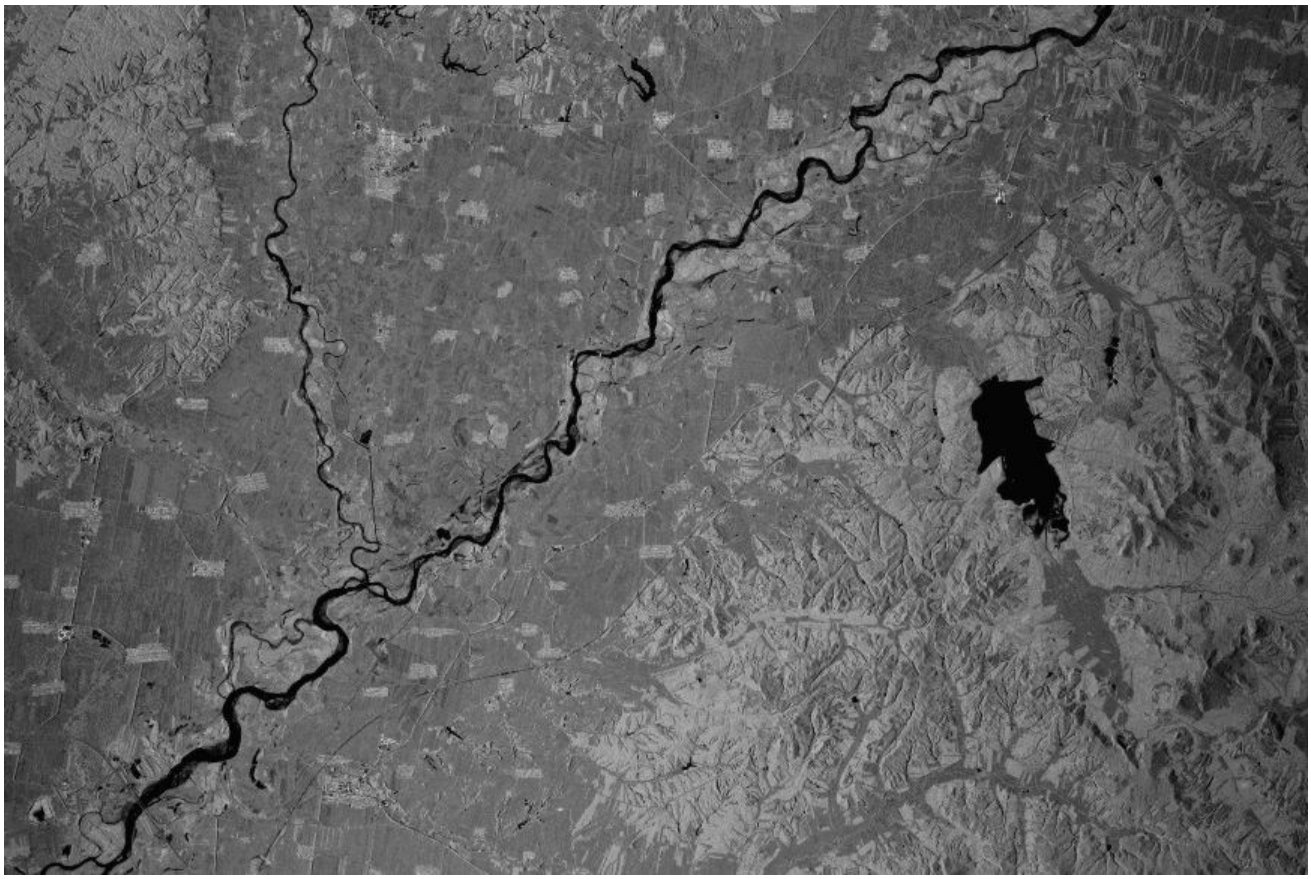

Figure 1 Mono-static HT1-A backscatter in slant range geometry.

2.2. Importing detected data in slant range geometry

Not available so far.

2.3. Importing geocoded / georeferenced data

Not available so far.

3. ASSESSMENT OF SOME CHARACTERISTICS OF HT1 STRIPMAP SLC DATA

3.1. Radiometric calibration and estimation of NESZ

We were (so far) not able to conduct an absolute radiometric calibration for HT1 data. Therefore, the data was not radiometrically calibrated in the SLC reading step. In the *multi_look* step we conducted a scaling to bring the backscatter to reasonable values. No validation with different satellite data or targets with known backscatter coefficients was done in our assessment.

Using dark areas (radar shadow and smooth water surfaces) we estimated a Noise Equivalent Sigma Zero value. Provided that we did not apply an accurate radiometric calibration there is a certain uncertainty but sufficient to find that the NESZ value is quite low (< -20 dB).

3.2. Point target characteristics

Considering several small, strong scatterers present in the scene we determined the following point target characteristics:

slant range resolution (3dB):	1.2 m
azimuth resolution (3dB):	2.0 m
peak_side_lobe_ratio:	< -20 dB

3.3. Geocoding

We generated a multi-look intensity image using 3 range and 2 azimuth looks and conducted a geocoding sequence, using the 1-arc-second Copernicus DEM. As part of the geocoding sequence a refinement was determined based on the offset between a simulated backscatter image (calculated based on the orbit data and the DEM) and the actual SAR backscatter.

The refinement statistics indicate for the offset estimates a very small standard deviation of below 0.7 multi-look pixel in both slant range and azimuth directions. For the data acquired in 2023, the determined range and azimuth refinement offsets were also small (< 5m).

3.4. RFI filtering

We did not identify narrow band RFI distortions in the HT1 data. We observed for one or maybe several locations in the scene an anomaly in the backscatter and the related spectrum determined using *dismph_fft* that we were not able to remove. A possible reason might be RFI.

4. HT1 MULTI-STATIC DIFFERENTIAL SAR INTERFEROMETRY (DINSAR)

4.1. Processing sequence used

We were able to test HT1 multi-static differential SAR interferometry using an HT1 multi-static acquisition over Yongfeng Town, Heilongjiang Province, China.

A flow chart of the main processing sequence used is shown in Figure 2. In the following, some of the steps are further discussed.

The monostatic scene was acquired by HT1-A. Three additional bistatic scenes were acquired by HT1-B, HT1-C, and HT1-D. The importing of all the four SLCs is done using the program *par_HT1_SLC*. For each SLC we estimated the Doppler Centroid parameters using *doppler_2d_SLC* and updated the SLC parameter files accordingly.

We selected the monostatic scene (HT1-A SLC) as the reference, generated a multi-look intensity image (MLI) with 3 range and 2 azimuth looks, and conducted a geocoding sequence using the Copernicus 30m global DEM. This also included the resampling of the DEM height into the MLI geometry. For the area of interest an oversampled DEM with about 3m sampling was used.

Next, we co-registered the 3 multi-static SLCs to the reference SLC. In this we used a sequence that also considers the terrain height (using *rdc_trans*). In *rdc_trans* the option for bistatic acquisitions is used. In this a refinement is done using intensity matching, to achieve a co-registration accuracy better than 0.2 SLC pixel.

The 4 acquisitions form 6 interferometric pairs with different spatial baselines with perpendicular components between about 60m and 500m. All the 4 acquisitions are quasi simultaneous, so the interferometric time difference is 0.

Then we calculated the orbital and topographic phase (*phase_sim_orb,* using the option for bistatic acquisitions) and the differential interferogram (*SLC_diff_intf*). The resulting differential interferogram have a high coherence. They all show a quite substantial overall phase trend that may be related to the exact geometry of the constellation, orbit movements, the geometric and phase model used in the bistatic SAR data focusing and the geometric model used in the simulation of the topographic and orbital phase (in the program *phase_sim_orb*). To subtract this overall low frequency phase term we first mask the forest and water areas (over the forest the phase clearly deviates from the low frequency residual orbital phase, over the water the phase is noisy). The masked phase is then spatially filtered (*fspf*) and unwrapped (*mcf*). This low frequency residual orbital phase is then subtracted (*sub_phase*) from the differential interferogram to get the "detrended" differential interferogram (Figure 3).

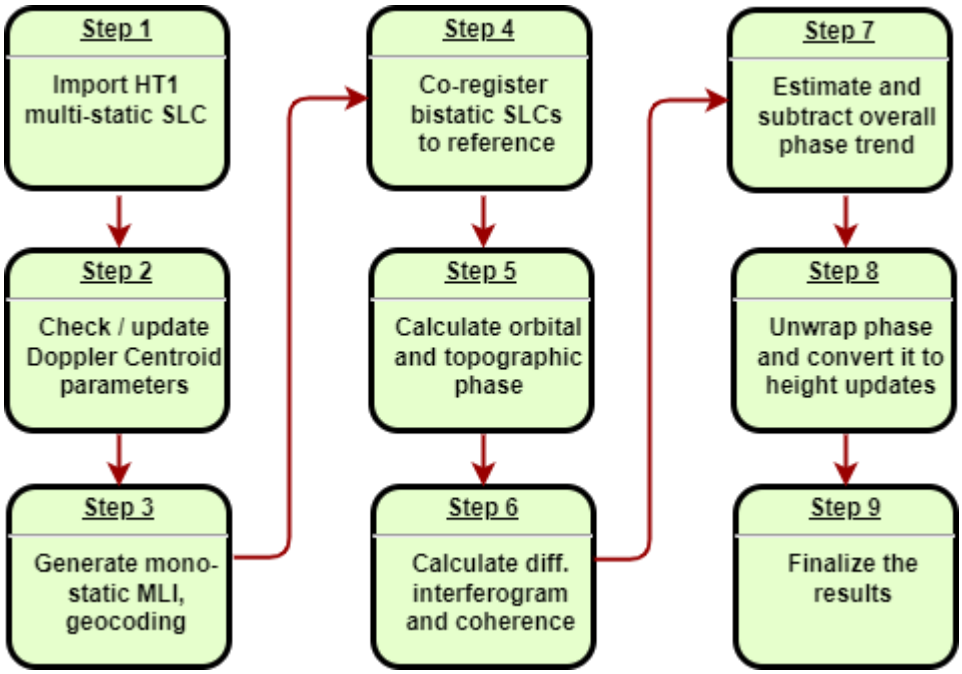

Figure 2 Flowchart of DInSAR processing sequence used.

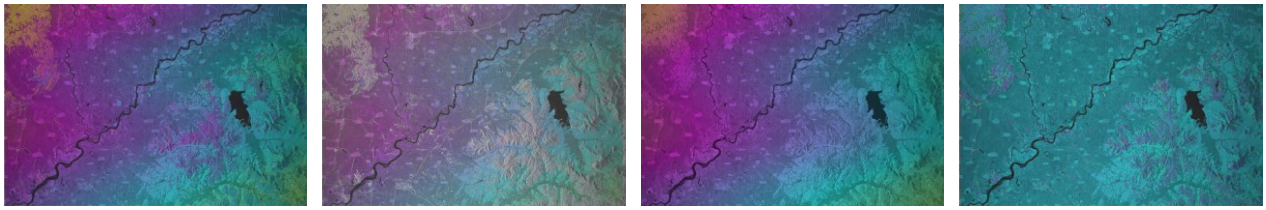

Figure 3 Differential interferogram detrending steps. From left to right the images show: the initial bistatic differential interferogram (including a substantial low frequency residual orbital phase), the masked differential interferogram, the filtered, unwrapped and interpolated masked interferogram (corresponding to our estimate of the low frequency residual orbital phase) and the detrended differential interferogram.

4.2. DEM update

The six detrended differential interferograms, small sections of three thereof are shown in Figure 4, are then spatially unwrapped using *mcf*. The height to phase sensitivity and height corrections relative to the Copernicus 1-arc-second DEM heights (which was used in the phase simulation) are then determined using *dh_map_orb*.

Further checking of the consistency of the height estimates, respectively of the phase unwrapping could be done to further improve the result. As a compromise between keeping the effort low, the method robust and achieving a high quality result we compared the height correction estimates and decided to simply use the median over the 6 estimates as the height correction determined. Furthermore, we masked the corrections over low coherence areas (water, radar shadow). It is clear that more advanced methods can be used – but it may get more complicated.

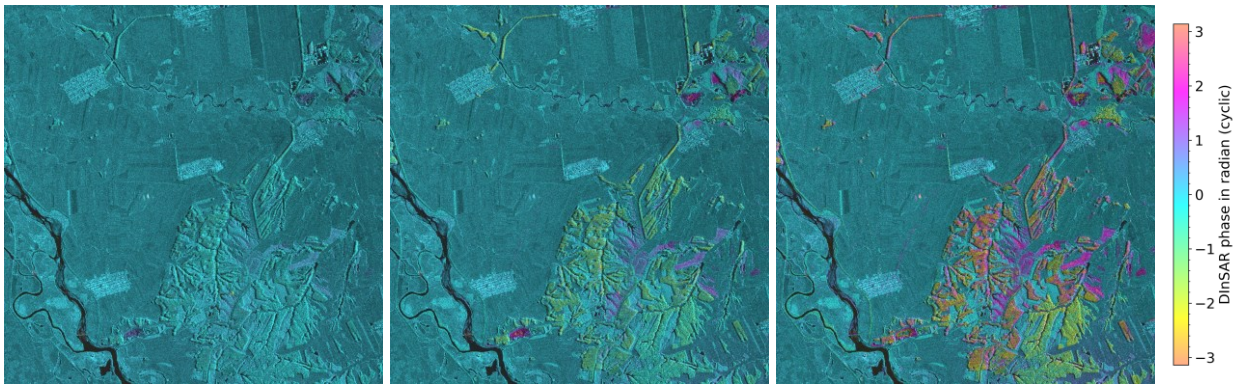

A-D, B⊥ -64m A-C, B⊥ -230m B-C, B⊥ -506m

Figure 4 5km x 5km sections of geocoded, detrended, multi-static HT1 differential interferograms. Below the image the sensor combination and the estimated perpendicular baseline are indicated.

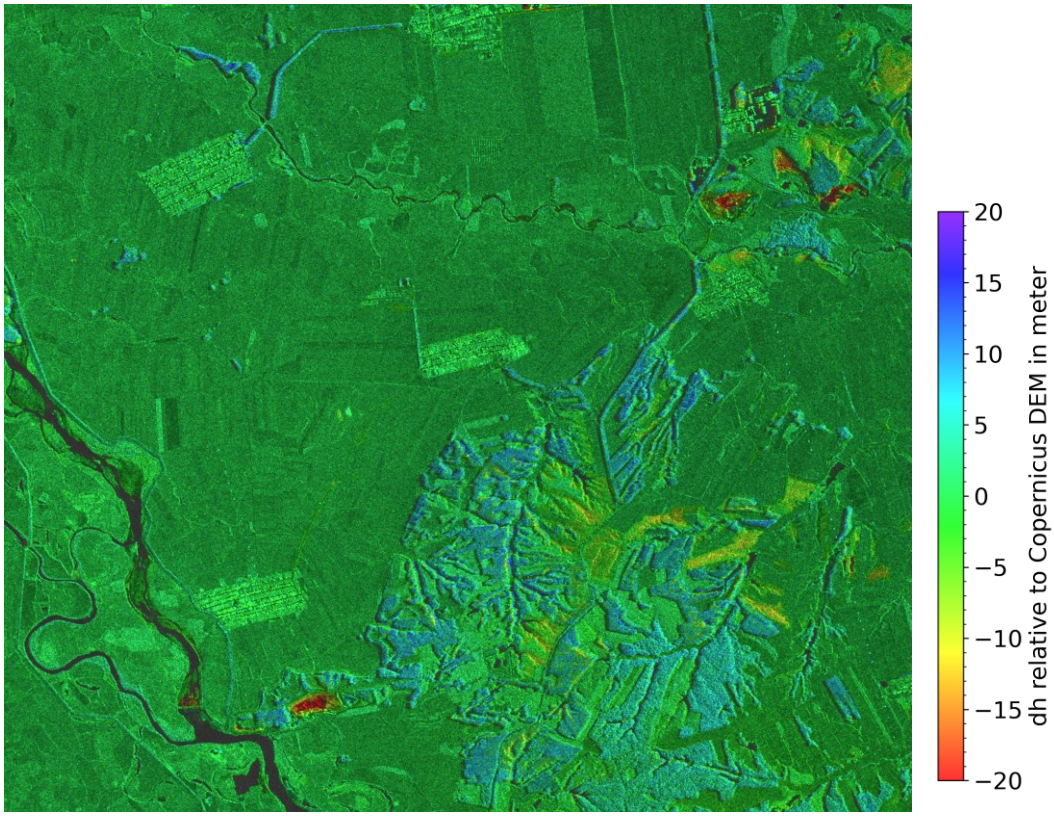

Figure 5 Height corrections relative to 1” Copernicus DEM heights (shown at 3m sampling, for an area of about 5km x 5km). The intensity of the image corresponds to the HT1A backscatter.

The determined height corrections are shown for a 5km x 5km area in Figure 5. Figure 6 shows for the same section shaded reliefs of the original (but spatially oversampled) Copernicus 1” DEM heights and the updated DEM generated using the HT1 multi-static data. It is obvious that the updated DEM has a clearly finer spatial scale (higher resolution). Corrections relate mainly to this resolution refinement, changes in the height obtained over forest (it seems the HT1 data provide higher forest heights than the Tandem-X results used to generate the Copernicus DEM), changes in

the forest (harvesting etc.), capturing smaller features as hedges along some smaller roads, and terrain changes (land excavation and fill). For large areas the result corresponds closely to the Copernicus DEM heights.

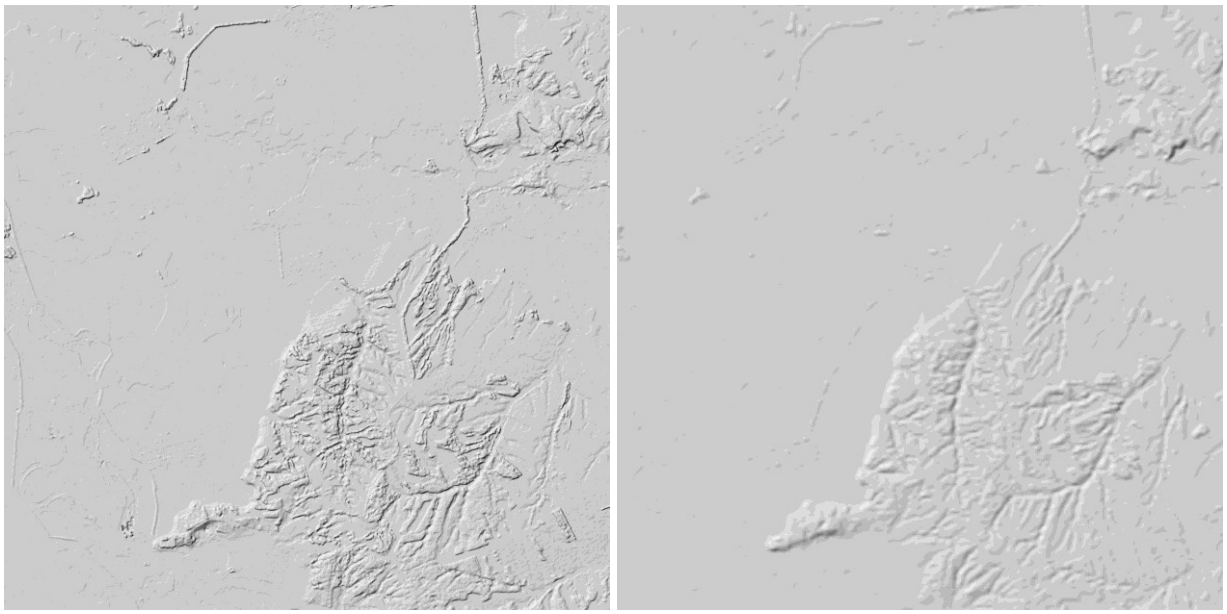

Figure 6 Shaded reliefs for the updated DEM section generated with HT1 multi-static DInSAR and the 1" Copernicus DEM (which was used as a starting point for the height map generation).

4.3. Multi-static coherence

Besides the multi-static differential interferometric phase the multi-static coherence provides interesting information. Figure 7 shows the multi-static coherence for 3 pairs with short to long baselines. Over forest we clearly observe a decrease of the coherence with increasing baseline. This behavior is known and can be used to estimate forest parameters as the forest stand height or biomass.

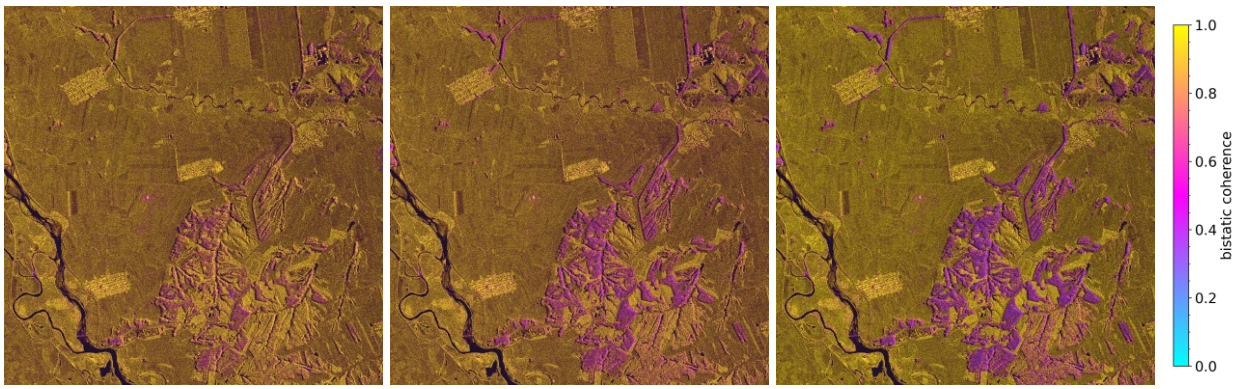

A-D, $B_\perp$ -64m A-C, $B_\perp$ -230m B-D, $B_\perp$ -339m

Figure 7 5km x 5km sections of geocoded, detrended, multi-static HT1 coherence. Below the image the sensor combination and the estimated perpendicular baseline are indicated. The SAR backscatter is used as image brightness.

4.4. Landcover information

In combination the SAR backscatter and coherence of a multi-static HT1 acquisition also provides interesting landcover information. Figure 8 shows an RGB color composite of the average coherence (red channel, using linear scaling), the average backscatter (green channel, using log scaling) and the backscatter variability between the different backscatter images (blue). The latter provides high values over water and radar shadow areas where the signal noise dominates, for the other areas the variation is quite low because of the high coherence between the data sets.

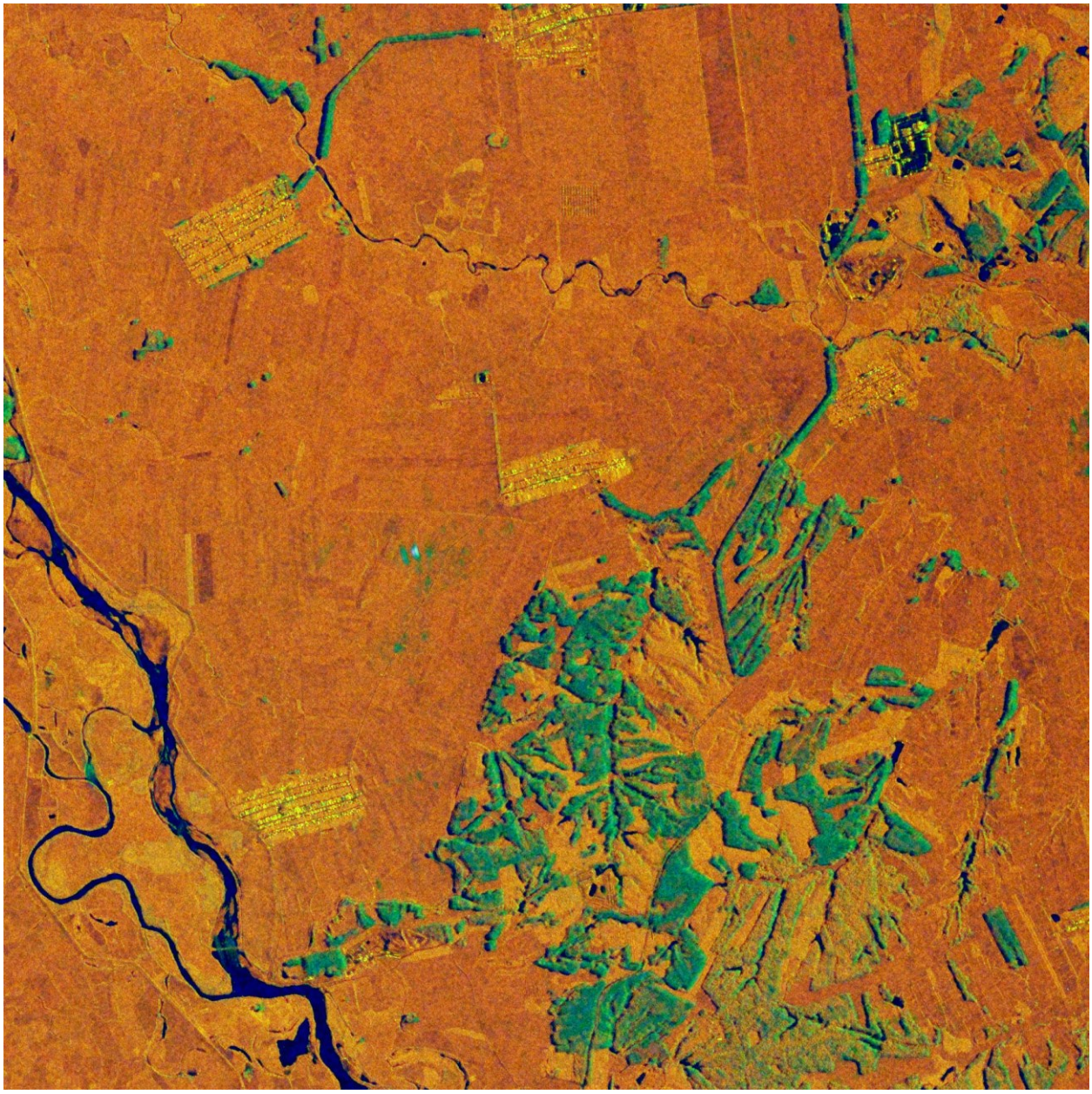

Figure 8 HT1 multi-static coherence product (RGB composite of average coherence (red), average backscatter (green) and the backscatter variability between multi-static scenes (blue).

4.5. Discussion

The multi-static SAR data acquired by HT1 is of high interest above all for the generation of high resolution digital elevation models. Acquiring simultaneously multiple pairs with a good variation of baselines has clear advantages over collecting multiple Tandem acquisitions over time, as done e.g. during the Tandem-X mission because of potential changes of the target (snow cover, vegetation growth, leaf on / leaf off, and terrain from landslides, mining construction work). Having 6 pairs available helps in resolving problems in the phase unwrapping, supports the quality control, and permits achieving a higher accuracy by combining the results.

Besides the interferometric phase the coherence is also of interest. In the case of volume scattering (forests, other vegetation, but also dry deserts, snow and ice) the coherence depends on the spatial baseline. This relation can be used to retrieve parameters on the mentioned volume scattering targets.

Using the data set (backscatter and coherence) also increases the potential for landcover classification, as compared to a single monostatic acquisition. Forest and water can quite easily be recognized.

We did not find evidence of a potential of along-track interferometry to identify moving targets and determine velocities – but we did not investigate this in detail.

We also investigated the presence of directional scattering. The different multi-static acquisitions have slightly different effective look directions. But the differences in the along track positions are only below 500m and so the angular difference is small (considering the slant range of about 700km). We did not observe many strong directional scattering effects.

5. ACKNOWLEDGMENT AND COPYRIGHTS

XingGuo Chen, of Beijing Di Kong Software Technology Co., Ltd, is acknowledged for providing access to the HT1 data used.